Topological transitions in ac/dc-driven open superconductor nanotubes

Vladimir M. Fomin (v.fomin@ifw-dresden.de)
Leibniz IFW Dresden
Roman O. Rezaev
Tomsk Polytechnic University
Oleksandr V. Dobrovolskiy
University of Vienna

Research Article

Keywords: condensed matter physics, nanostructure, superconducting

Posted Date: October 19th, 2021

DOI: https://doi.org/10.21203/rs.3.rs-991951/v1

Topological transitions in ac/dc-driven open superconductor nanotubes

Vladimir M. Fomin[1,2,3*], Roman O. Rezaev[4], Oleksandr V. Dobrovolskiy[5]

[1] *Institute for Integrative Nanosciences, Leibniz IFW Dresden, Helmholtzstraße 20, D-01069 Dresden, Germany*

[2] *Laboratory of Physics and Engineering of Nanomaterials, Department of Theoretical Physics, Moldova State University, strada A. Mateevici 60, MD-2009 Chisinau, Republic of Moldova*

[3] *Institute of Engineering Physics for Biomedicine, National Research Nuclear University "MEPhI", Kashirskoe shosse 31, 115409 Moscow, Russia*

[4] *Tomsk Polytechnic University, Lenin av. 30, 634050 Tomsk, Russia*

[5] *SuperSpin Lab, Nanomagnetism and Magnonics, Faculty of Physics, University of Vienna, Währinger Str. 17, 1090 Vienna, Austria*

* E-mail: v.fomin@ifw-dresden.de

Abstract

Extending of nanostructures into the third dimension has become a major research avenue in condensed-matter physics, because of geometry- and topology-induced phenomena. In this regard, superconducting 3D nanoarchitectures feature magnetic field inhomogeneity, non-trivial topology of superconducting screening currents and complex dynamics of topological defects. Here, we investigate theoretically topological transitions in the dynamics of vortices and phase slips in open superconductor nanotubes under a modulated transport current. Relying upon the time-dependent Ginzburg-Landau equation, we reveal two distinct voltage regimes when (i) a dominant part of the tube is in the normal or superconducting state and (ii) the complex interplay between vortices, phase slips and screening currents determines a rich FFT voltage spectrum. Our findings allow for unveiling the distributions of the superconducting order parameter in open nanotubes via recording time-dependent induced voltage and for controlling these states by using superimposed dc and ac transport currents.

1. Introduction

Modern advances of high-tech fabrication techniques have allowed for generating geometrically and topologically nontrivial manifolds at the nanoscale, which determine novel, sometimes counterintuitive electronic, magnetic, optical and transport properties of such objects and unprecedented potentialities for design, functionalization and integration of nanodevices due to their complex geometry and non-trivial topology [Fomin18a,Fomin18b]. Within the ongoing investigations of curvilinear geometry, ranging from solid-state physics over soft-matter physics, chemistry and biology to mathematics, a plethora of fascinating domains have emerged such as curvilinear nematics, curvilinear entities of cell biology, curvilinear semiconductors, superfluidity, optics, plasmonics, magnetism and

superconductivity [Makarov2021], relying upon self-rolled 3D micro- and nanoarchitectures [Prinz00, Schmidt01a]. Within a holistic approach, the effects of rolling up have been analyzed for semiconductor, superconductor, and magnetized micro- and nanoarchitectures, catalytic tubular micromotors and optical waveguides [Fomin21].

Rolling up a planar film into a tubular structure brings about two fundamental aspects: (i) The direction of the externally applied magnetic field is varying with respect to the normal to the sample surface, that is, the in-plane and out-of-plane field components become strongly inhomogeneous. (ii) The superconducting screening currents can evolve from a singly-connected Meissner loop to more complex patterns, with a multiply-connected topology. Accordingly, hybridization of reduced dimensionality in a superconductor with curved geometry and non-trivial topology is a rich source of emerging physics. For instance, measurements of the magnetoresistance in superconductor cylinders [Little62] and loops [Moshchalkov95] revealed fluxoid quantization and a huge impact of nanostructuring on the normal-superconducting phase boundary. Curvature was found to be the key factor to control the depression of the critical temperature in thin superconductor cylindrical shells as a function of the angle between the axis of the cylinder and the magnetic field [Tinkham63, Meservey72]. The coexistence of the Meissner state with various vortex patterns in thin superconductor spherical shells [Gladilin08] was shown to drive the phase transition to higher magnetic fields [Tempere09]. The multiple periodicity of magnetoresistance observed in YBCO nanoscale rings [Carillo10] pointed to the existence of concentric vortex structures with non-uniform vorticity [Zhao03]. In high-temperature superconducting films patterned into a network of nanoloops, interplay between thermally excited moving vortices and the oscillating persistent current was revealed to lead to magnetoresistance oscillations [Sochnikov10].

The key pathways in fabrication of complex superconductor 3D nanoarchitectures are based on the advanced 3D roll-up self-organization [Lösch19] and nanowriting techniques using focused electron-beam [Pacheco20] or focused ion-beam induced deposition [Cordoba19] (FEBID and FIBID, respectively). For instance, the recent finding of the suppression of the critical current of a superconducting W-C-FIBID nanostructure by applying an electric field in its vicinity [Orus21] opens up a rich realm of unexplored phenomena induced by the interplay between the geometry of nanostructures and applied fields. Ultra-fast vortex motion in Nb-C-FIBID microstrips at velocities exceeding 10 km/s [Dobrovolskiy20] is another example of unique phenomena offered by direct-write superconductors [Porrati19].

A systematic study of rolled-up superconductor nano- and microarchitectures (tubes and helices) has been performed in the last decade [Fomin21]. Strain-driven self-assembly of rolled-up architectures on the nano- and microscale allows for the fabrication of Swiss-roll-shaped micro- and nanotubes with superconductor layers (e.g. InGaAs/GaAs/Nb). Those hybrid structures open hitherto unprecedented possibilities for experimental investigations of vortex matter in superconductors with curved geometries. The dynamics of vortices in such structures are described by two characteristic times: the period of

nucleation of vortices at one edge of the structure and the duration of motion of a vortex along the structure. Numerical modeling within the time-dependent Ginzburg–Landau (TDGL) approach revealed that the curved geometry governs the dynamics of vortices in the presence of transport currents in open superconductor micro- and nanotubes subject to a magnetic field orthogonal to the axis [Fomin12a]. Synergetic effects of the shape and dimensions on both equilibrium and dynamical vortex distributions cause drastic changes of vortex patterns, that leads to a non-monotonic dependence of the characteristic times on the magnetic field. Being of the order of several microvolts in magnitude, the voltage induced by the moving vortices in open tubes at the micrometer scale can be detectable by modern equipment. The detection of the tube curvature effects on vortex dynamics remains feasible in the presence of pinning centers [Rezaev14]. At the applications-oriented facet, open microtubes can be viewed as tunable superconducting fluxon generators for emerging fluxon-based information technologies.

At a certain value of the magnetic field, which depends on the geometry of the tube, collective phenomena lead to the bifurcation of vortex trajectories [Rezaev15]. Using inhomogeneous transport current in a microtube with multiple electrodes allows for vortex removal from certain regions of the tube, which is of practical interest, for example, in order to suppress the 1/*f*-noise due to the activated hopping of trapped vortices and thus to extend the operation regime of superconductor-based sensors to lower frequencies. [Rezaev16].

Theoretical investigations of the superconducting state in helical coils at the micro- and nanoscale are performed within the TDGL approach [Fomin17]. The pattern and number of vortices in a stationary distribution are determined by their confinement to the ultrathin helical coil and can therefore be efficiently controlled by the spiral stripe width and the spiral pitch distance for both dense and sparse coils. Quasi-degeneracy of vortex patterns is manifested in the helical coil when the number of vortices is incommensurable with the total number of half-turns. The obtained results demonstrate perspectives for tailoring both equilibrium and non-equilibrium properties of vortices in curved superconductor micro- and nanoarchitectures.

Rolling up superconductor Nb nanomembranes into open tubes allows for a new, highly correlated vortex dynamics regime. The induced voltage as a function of the magnetic field provides information about the vortex pattern. In particular, an increase of the number of vortex chains in the tube results in a six-fold decrease of a slope of the induced voltage as a linear function of the magnetic field [Rezaev19]. The topological transition between the vortex-chain and phase-slip regimes [Rezaev20] opens up new perspectives for the advanced technological applications of self-rolled superconductor nanoarchitectures, such as for high-performance detectors and sensors, energy-storage components, quantum computing and microwave radiation detection.

The numerical modeling of vortex dynamics was also performed for finite-thickness open micro- and nanostructures [Smirnova2020]. A decrease of the distance between the upper and lower 500-nm-thick plates of a C-shaped nanostructure down to 30 nm enhances the interaction between vortices in the both

plates, what causes slowing down of vortex dynamics. This analysis provides a justification for the 2D approximation used for tubes under analysis in the present paper, since the membrane's thickness d~50 nm is substantially smaller than both, the effective penetration depth for the Nb membrane and the tubes's diameter ~800 nm.

The dynamics of vortices under an ac current exhibit a rich variety of dynamical regimes, which are determined by both, the ac amplitude and the ac frequency. Distinct from the translational motion under the action of a dc current, an ac current causes oscillatory motion of vortices [ShklovPompeo08, Dobrovolskiy15a]. However, the dynamics of vortices in superconductor 3D micro- and nanostructures have been so far studied in the regimes of dc or ac currents separately. At the same time, from previous studies of planar superconductor films, it is known that a combination of dc and ac current drives can give rise to novel phenomena, such as dc/ac quantum interference [Fiory71, Martinoli75], rectified voltage and its reversal [Shklovskij14, Dobrovolskiy15b], and peculiarities in the microwave power absorption [Dobrovolskiy20b]. Based on the above findings, a boost to development of nanoelectronics is expected by virtue of properties of curved superconductor structures under a combined dc+ac transport current, which are the subject of this report.

Here, we study numerically the (dc+ac)-driven dynamics of topological defects in open superconductor nanotubes. The theoretical treatment is carried out relying upon the solution of the TDGL equation. We demonstrate that the (dc+ac)-biased nanotubes in a magnetic field orthogonal to their axis manifest a plethora of inhomogeneous states, with distinct time−voltage characteristics. We analyze the effects of magnetic field, dc magnitude, ac amplitude and frequency on the patterns of topological defects and reveal two regimes in the voltage response of the nanotubes. The first regime is characterized by a pronounced first harmonic in the FFT spectrum of the induced voltage at the ac current frequency. This regime occurs when the dominant area of the open tube is in the superconducting or normal state. The second regime is accompanied by a rich voltage FFT spectrum, because of the interplay between the dynamics of superconducting vortices or phase slips and the dynamics induced by the ac current. These findings open a pathway towards experimental unveiling of distributions of the superconducting order parameter in open nanotubes via recording the time-dependent induced voltage and manipulation of these states by using a modulated transport current.

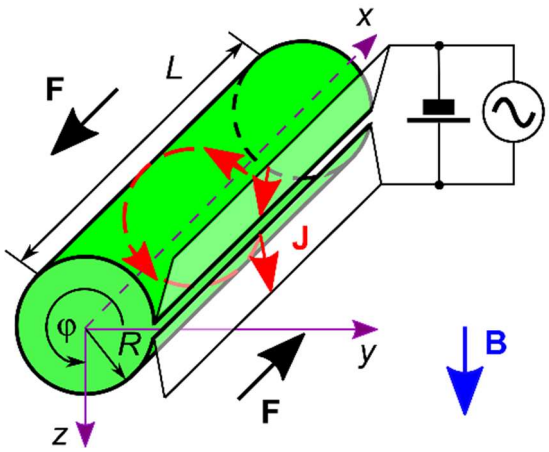

Fig. 1. Geometry of the considered system. An open superconducting nanotube is in a magnetic field with induction **B** directed perpendicular to the tube axis. A combination of the dc and ac transport currents **J** flows along the generatrix of the tube and exerts the driving force **F** on moving vortices. The voltage associated with the dynamics of topological defects in the tube is measured between two electrodes attached at both sides of the slit.

2. Model

We consider an open superconductor Nb tube with dimensions implied by the roll-up technology: length L = 5 μm, radius R = 400 nm; the tube is made from a 50 nm-thick film [Thurmer08, Thurmer10]. Figure 1 shows a scheme of the system under consideration. Two paraxial electrodes are attached to both edges of the slit in order to apply a transport current. The width of the slit is supposed to be much smaller compared to the circumference $2\pi R$. The electrodes extend through the entire slit edges. The system is placed in the magnetic field $\boldsymbol{B} = B\boldsymbol{e}_z$, which induces screening superconducting currents circulating at each half-tube [Fomin12a]. The temperature of the tube is taken T=0.77T_c, where T_c is the critical temperature.

The superconducting state of the Nb tube with parameters presented in Table 1 is described by the TDGL equation for the complex-valued order parameter ψ [Tinkham96, Gropp96] in the dimensionless form:

$$\frac{\partial\psi}{\partial t} = \left(\frac{\nabla}{\kappa} - i\boldsymbol{A}\right)^2 \psi + (1 - |\psi|^2)\psi - i\kappa\varphi\psi, \qquad (2.1)$$

where φ is the electric scalar potential. The boundary conditions

$$(\nabla - i\mathbf{A})\psi|_{n,\text{boundary}} = 0 \qquad (2.2)$$

imply zero value of the normal component of the superconducting current at the edges of the system without electrodes. The scalar potential φ is found as a solution of the Poisson equation coupled with TDGL equation (2.1):

$$\Delta\varphi = \frac{1}{\sigma}(\nabla, \boldsymbol{j}_{\text{sc}}), \qquad (2.3)$$

Table 1. Physical and geometrical parameters of the Nb films used for simulation

Parameter	Denotation	Value	Refs.
	λ_0	43 nm	[Dobrovolskiy20c]
	ξ_0	312.3 nm	Calculated after [Dobrovolskiy20c]
Relative temperature	T/T_c	0.77	-
Resistivity	ρ_0	70.2 μΩ·cm	[Dobrovolskiy20c]
Mean free electron path	$l = 3.72 \times 10^{-6}\ \mu\Omega\ \mathrm{cm}^2/\rho_0$	0.53 nm	[Mayadas1972]
Effective penetration depth	$\lambda = \lambda_0 \sqrt{\frac{\xi_0}{2(1 - T/T_c) \times 1.33l}}$	1.334 □m	(4.26a), (4.26b) [Tinkham96]
Coherence length	$\xi = 0.855 \sqrt{\frac{\xi_0 l}{1 - T/T_c}}$	22.93 nm	(4.24b) [Tinkham96]
GL parameter	$\kappa = \lambda/\xi$	58.18	(4.27) [Tinkham96]
Fermi velocity	v_F	6×10^5 m/s	[Gubin2005]
Thickness of the film	d	50 nm	-
Diffusion coefficient	$D = lv_F/3$	1.06×10^{-4} m^2/s	
Normal conductivity	$\sigma = l/[3.72 \times 10^{-16}(\Omega \cdot \mathrm{m}^2)]$	1.42 $(\mu\Omega \cdot \mathrm{m})^{-1}$	[Dobrovolskiy12]

where the superconducting current density is defined as $\mathbf{j}_{sc} = \frac{1}{2i\kappa}(\psi^* \nabla\psi - \psi\nabla\psi^*) - \mathbf{A}|\psi|^2$ and σ is the normal conductivity. The transport current density $j_{\mathrm{tr}}(y) = \mathrm{const} \equiv j_{\mathrm{tr}}$ is imposed via the boundary conditions for Equation (2.3) at the edges, to which electrodes are attached: $(\mathbf{n}, \nabla)\varphi|_{\mathrm{electrode}} = -\left(\frac{1}{\sigma}\right) j_{tr}$. The transport current density is modulated by the ac component with frequency f:

$$j_{\mathrm{tr}}(t) = j_0 + j_1 \sin(2\pi f t). \qquad (2.4)$$

The vector potential components $A_s(s, y)$ and $A_y(s, y)$ (where $s = R\theta$) are chosen in the Coulomb gauge: $A_s(s, y) = 0; \quad A_y(s, y) = BR\cos\left(\frac{s}{R}\right)$. The set of equations (2.1) and (2.3) is solved

numerically, based on the link variables technique [Gropp96]. The relaxation method is used with a random initial distribution $\Psi(s,y)$ of the order parameter. In the presence of magnetic field ($B > B_{c1}$) and transport current, the order parameter evolves to a quasi-stationary state, which is characterized by the periodic vortex nucleation/denucleation at the edge domains with the highest/lowest value of the normal to the surface component of magnetic field [Gropp96, Kato93, Kogut79, Saad96]. Vortices are moving paraxially along the tube and generate the electric field, which is directed oppositely to the transport current density [Fomin12a]. Finally, the induced voltage $U(t)$ averaged over the electrode length is obtained.

3. Dynamics of the superconducting state under a modulated transport current

Under a transport current density of Equation (2.4), which consists of a dc component j_0 superposed with an ac component of frequency f and amplitude j_1, so that the modulation depth is j_1/j_0, the dynamics of the order parameter in an open tube reveals a modulation reflecting various stages of evolving topological defects and transitions between them. In what follows, we begin with a description of the evolution of the order parameter during one ac cycle and then consider the effects of each of the driving parameters on the voltage response.

3.1 Evolution of the order parameter and the induced voltage

The superconducting order parameter developing from a random initial state, after some relaxation, achieves a quasi-stationary state, which evolves nearly periodically between the regimes illustrated in Fig. 2. The time-dependent induced voltage is shown in Supplementary Figure 1. The evolution of patterns of topological defects is presented in more detail in Supplementary Video 1. For definiteness, in Fig. 2 we consider the key stages of the evolution of the modulus and phase of the superconducting order parameter in nanotube 20210419B at B = 2mT for the modulation depth $\frac{j_1}{j_0} = 0.5$ at f = 0.6 GHz: (i) When the modulated transport current acquires the lowest values (at 2.95 ns) there are only a few individual vortices moving in the two half-cylinders in the opposite directions under the influence of the Magnus force, while the induced voltage U is close to zero. In this case, the potential drops in narrow regions near the banks, where a transition from the normally-conducting leads to the superconducting tube occurs. During some time till the next stage, only different constellations of moving vortices determine small variations of $U(t)$. (ii) A state with two phase-slip regions close to the banks of the slit is appearing at 3.52 ns, when the induced voltage ranges between 0.54 mV and about 1 mV. The two phase-slip regions can also be identified via the phase portrait of the superconducting state. (iii) The above-described phase-slip regions extend from the banks of the slit and induce the main voltage drop. Precursors of further phase slips in the central regions of the both half-cylinders as well as in the region opposite to the slit occur starting at 3.6 ns, so that the total induced voltage ranges between 1.18 mV and about 2 mV. (iv) When the modulated transport current acquires the highest values at around 4 ns,

Table 2. Parameters of the simulated open tubes with $R = 400$ nm, $L = 5$ μm

Name of structure	B, mT	j_0, 10^9 Am^{-2}	f, GHz	$\frac{j_1}{j_0}$	$\frac{T}{T_c}$	$U_0, \mu V$	$\frac{U_1}{U_0}$	$\frac{U_2}{U_0}$	$\frac{U_3}{U_0}$
20210420A	0	2.1048	0.6	0.5	0.77	1346	1.127	0.118	0.094
20210419B	2	2.1048	0.6	0.5	0.77	1318	0.985	0.172	0.068
20210219B	2	2.1048	3.0	0.5	0.77	1892	0.412	0.072	0.051
20210219A	2	2.1048	6	0.5	0.77	995	0.512	0.098	0.030
20210325A	4	2.1048	0.6	0.3	0.77	998	1.111	0.146	0.103
20210306A	4	2.1048	0.6	0.5	0.77	1474	1.046	0.035	0.131
20210320A	4	2.1048	0.6	0.8	0.77	2056	1.053	0.033	0.093
20210320B	4	2.1048	0.6	1.0	0.77	2163	1.143	0.073	0.111
20210311A	6	2.1048	0.6	0.5	0.77	2026	0.730	0.066	0.086
20210419C	10	2.1048	0.6	0.5	0.77	1772	0.796	0.081	0.066
20210217C	2	2.4556	60	1.0	0.77	3750	0.295	0.001	0.036
20210217D	6	2.4556	60	1.0	0.77	3826	0.289	0.001	0.035
20210217E	10	2.4556	60	1.0	0.77	3750	0.314	0.000	0.038
20210927E	0	2.1048	60	0.5	0.77	147.1	1.444	0.093	0.093
20210927A	2	2.1048	60	0.5	0.77	149.7	1.008	0.074	0.074
20210927B	4	2.1048	60	0.5	0.77	153.4	1.286	0.110	0.109
20210927C	6	2.1048	60	0.5	0.77	171.3	1.213	0.093	0.093
20210927D	10	2.1048	60	0.5	0.77	256.6	0.621	0.050	0.050
20211002D	2	2.280	60	0.5	0.77	255,0	1.018	0.016	0.062
20210927E	2	2.324	60	0.5	0.77	330.1	0.696	0.011	0.068
20211002F	2	2.368	60	0.5	0.77	2243	0.142	0.001	0.011
20211002G	2	2.412	60	0.5	0.77	2427	0.123	0.001	0.008
20210929F	2	2.1048	1	0.5	0.77	1274	1.014	0.071	0.097
20210929A	2	2.1048	10	0.5	0.77	237	1.073	0.194	0.082
20210929B	2	2.1048	20	0.5	0.77	332	0.550	0.030	0.028

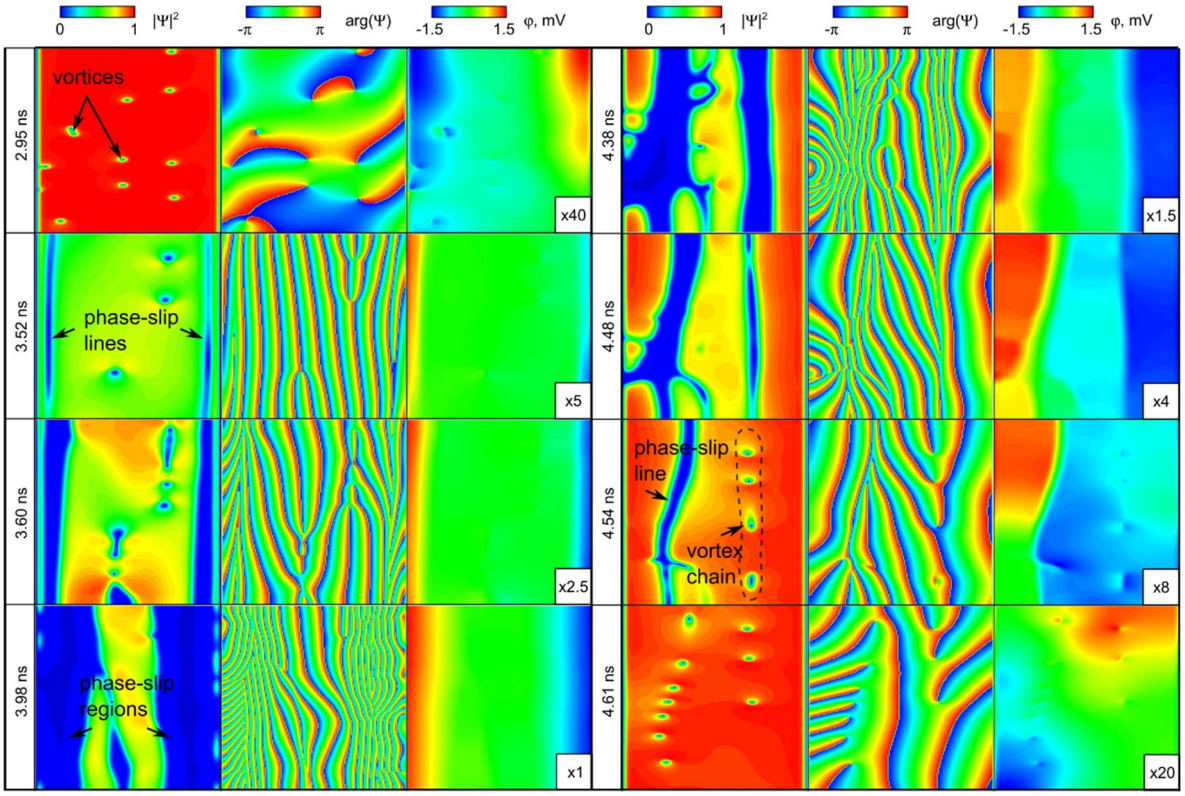

Fig. 2. Patterns of topological defects in the low-frequency regime. Key stages of a period of evolution of the modulus and phase of the order parameter and the electric potential for B=2 mT at $\frac{j_1}{j_0} = 0.5$ and f = 0.6 GHz (refer to nanotube 20210419B in Table 2). The sizes of all panels (height × width) are equal to $L \times 2\pi R$ (length × circumference of the tube), respectively. The evolution is illustrated in Supplementary Video 1.

the phase slips from stage (ii) become the widest ones, while the phase slips from stage (iii) fade out. The total induced voltage rises up to its maximal value 2.9 mV at 3.98 ns, when the transport current is the strongest. At about 4.24 ns (not shown in Fig. 2), the order parameter begins to reenter first the region opposite to the slit. The total induced voltage begins to decay down to 2.39 mV. (v) A new *azimuthal* phase-slip region is developing next to the old *paraxial* phase-slip regions. The phase-slip regions of regime (ii) depart from the banks of the slit and become narrower at 4.38 ns. The total induced voltage continues to decay down to 1.5 mV. (vi) The phase-slip regions of both types can be still seen at 4.48 ns, when the total induced voltage decays down to about 0.7 mV. Interestingly, the azimuthal phase-slip regions are clearly reflected in the distribution of the induced potential. (vii) At 4.54 ns one of them is already split into a chain of individual vortices, while the other one still survives, but becomes very narrow. The total induced voltage decays down to 0.24 mV. (viii) At about 4.61 ns, only two chains of vortices moving in the two half-cylinders in the opposite directions are present, which induce the voltage close to zero. The period of the order-parameter dynamics Δt = 1.66 ns, which accurately corresponds to the frequency of the modulated transport current, f = 0.6 GHz, is completed. The time-dependent voltage $U(t)$ (see Supplementary Figure 1) has a rich harmonic spectrum supporting the fact that the voltage response is a *nonlinear* function of the transport current. The modulation depths

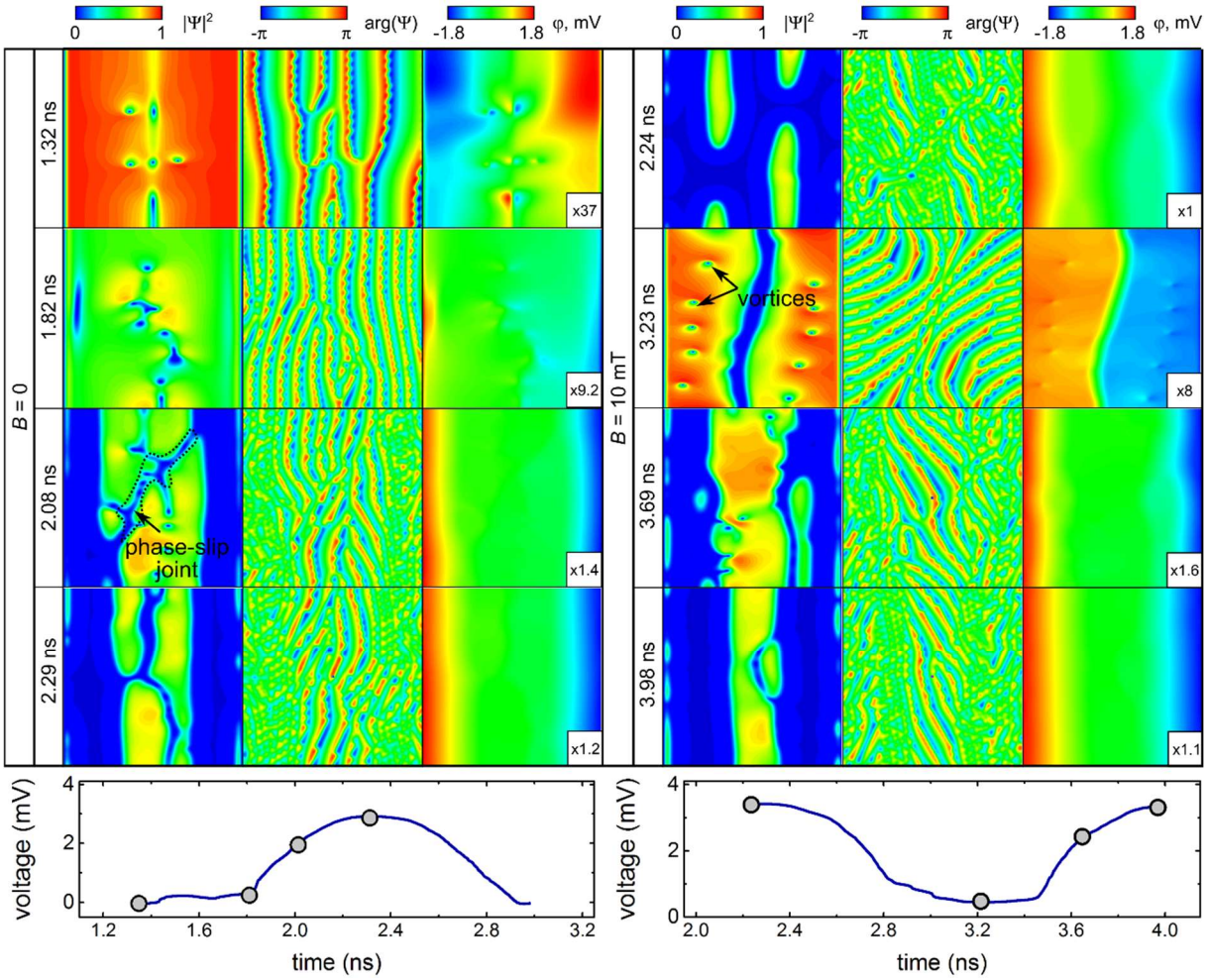

Fig. 3. Effect of the magnetic field on the dynamics of topological defects. Evolution of the modulus and phase of the order parameter, electric potential, and time-dependent induced voltage for B =0 (left panels) and B=10 mT (right panels) at $\frac{j_1}{j_0} = 0.5$ and f = 0.6 GHz. The evolution is illustrated in Supplementary Video 1.

of $U(t)$ at three first harmonics are reported in Table 2. Remarkably, the modulation depth of $U(t)$ at the first harmonic has a magnitude almost twice as large as the modulation depth of the transport current.

3.2 Effect of the magnetic field

In the same structure, for the same driving parameters at zero magnetic field (Fig. 3, left column), the key difference from the previous case is that the vortices, occurring at the weakest transport current, like those at 1.32 ns, do not move in some ordered way, so that the minimum value of the induced voltage is close to zero. The occurrence of phase-slip regions at 1.82 ns gives rise to an induced voltage of 0.3 mV, which increases to 3 mV at 2.29 ns, when the transport current is the strongest, due to widening of the phase slips from the banks of the slit as well as due to the occurrence of new phase slips in the region opposite to the slit. Interestingly, at 2.08 ns a further phase slip emerges, which *joins both halves* of the cylinder. This emphasizes the fact, that we are dealing with the states of holistic nature, which belong to the whole superconductor open tube, rather than to its halves separately.

For a magnetic field increased to 10 mT (Fig. 3, right column), the average induced voltage increases from 1.32 mV to 1.77 mV, the modulation depth at the first harmonic decreases from 0.985 to 0.796 and at the second harmonic decreases from 0.172 to 0.081: the second and higher harmonics decay by intensity. The minima of the induced voltage correspond to a coexistence of vortices and two phase-slip regions close to the region, opposite to the slit, e.g., at 3.23 ns, 3.98 ns and 5.00 ns. The maxima of the induced voltage contain wide *interconnected* phase-slip regions near the banks of the slit and opposite to the slit at 2.24 ns and near the banks of the slit at 3.98 ns and 5.58 ns. Interestingly, as clear from the phase dynamics, while the vortices in the major phase-slip areas extend mainly in the *paraxial* direction, the interconnects correspond to the vortices moving predominantly in the *azimuthal* direction. This trend gradually develops when increasing the magnetic field B from 2 to 6 mT.

3.3 Effect of the modulation depth of the transport current

In the following discussion we consider the same nanotube in a magnetic field B of 4 mT (Fig. 3a).When the modulation depth of the transport current is relatively small, $\frac{j_1}{j_0} = 0.3$, the minimal induced voltage is as high as 0.5 mV at 3.38 ns and 40 μV at 4.77 ns, when there exist only a few vortices in the tube, because the transport current even at minima has a significant magnitude. The maximal induced voltage is about 2.5 mV at 4.02 ns and 2.25 mV at 5.65 ns, when there are two clearly expressed phase-slip regions close to the banks of the slit. Correspondingly, the average voltage is about 1 mV and the modulation depth of the first harmonic is as large as 1.11. When the modulation depth of the transport current is increased up to 0.5, the average induced voltage increases to 1.47 mV, while the modulation depth of the first harmonic of the induced voltage slightly decreases to 1.05 and the second harmonic significantly decays. The maximal values of the induced voltage reach 4 mV at 3.84 ns and 4.2 mV at 5.65 ns, when two phase-slip regions develop close to the banks of the slit. At distinct from the smaller values of the modulation depth of the transport current, the minimal values vanish at 4.66 ns and 6.38 ns with two very narrow phase-slip regions opposite to the slit. When the modulation depth of the transport current is further increased up to 0.8, the average induced voltage further increases to 2.06 mV, while the modulation depth of the first harmonic of the induced voltage further slightly decreases to 1.05. The maximal values of the induced voltage reach 4 mV at 3.84 ns and 4.2 mV at 5.65 ns (with two wide phase-slip regions in both half-tubes). At distinct from the smaller values of the modulation depth of the transport current, the minimal values *vanish* at 4.66 ns and 6.38 ns (with only a few vortices). Finally, when the modulation depth of the transport current is increased up to 1.0, the average induced voltage further increases to 2.16 mV, while the modulation depth of the first harmonic of the induced voltage increases to 1.14. The maximal values of the induced voltage reach 4.7 mV at 5.64 ns and 8.2 mV at 7.29 ns (with two wide phase-slip regions in both half-tubes). The minimal values of the induced voltage vanish at 6.43 ns and 8.30 ns (with only a few vortices).

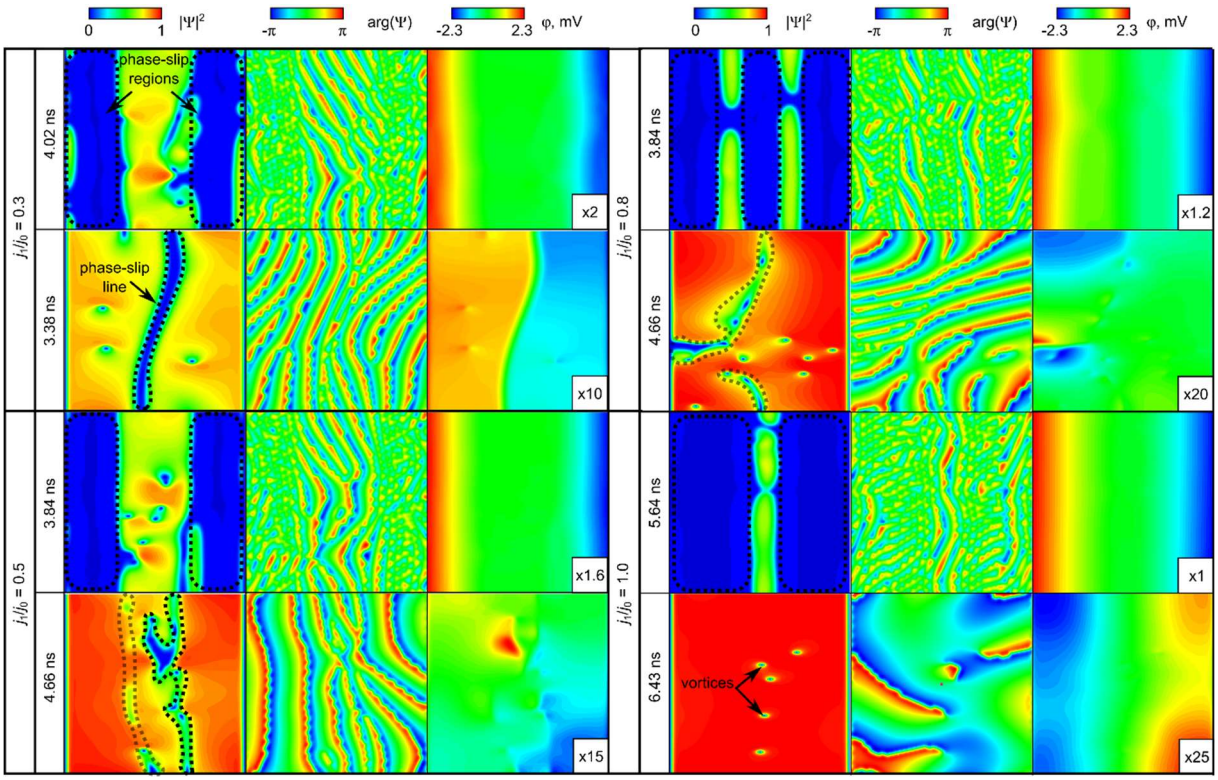

Fig. 4. Effect of the modulation depth of the transport current. Evolution of the modulus and phase of the order parameter and electric potential for $B = 4\text{mT}$, $f = 0.6$ GHz for a series of modulation depths $\frac{j_1}{j_0} = 0.3, 0.5, 0.8, 1$. The evolution is illustrated in Supplementary Video 2.

3.4 Effect of the ac frequency

The main effect of the ac frequency (Fig. 5) consists in the development of a sequence of harmonics in the response of the induced voltage. The modulation depth of the first harmonic of the induced voltage constitutes 0.98, 0.41 and 0.51 for the ac current frequencies 0.6 GHz, 3 GHz and 6 GHz, respectively. The fact, that for the ac current frequency 0.6 GHz it is significantly higher than the modulation depth 0.5 for the transport current reflects the dramatic transitions between states with various configurations of superconducting vortices and phase-slip states. The stationary state periodically changes with time between states with normal phase almost everywhere, which provide the maximal voltage of the order of 3 mV, and states with a predominant superconducting state except two regions of suppressed superconductivity in both half-cylinders, which provide the minimal voltage close to zero in the second and further minima. Since we observe a modulation of the pattern of the superconducting order parameter, the voltage as a function of time clearly deviates from a sinusoidal function.

For the higher ac current frequencies 3 GHz and 6 GHz, the modulation depth of the first harmonic of the induced voltage is approximately as large as the modulation depth for the transport current. The modulated stationary state of the superconductor open tube is a coexistence of the extended

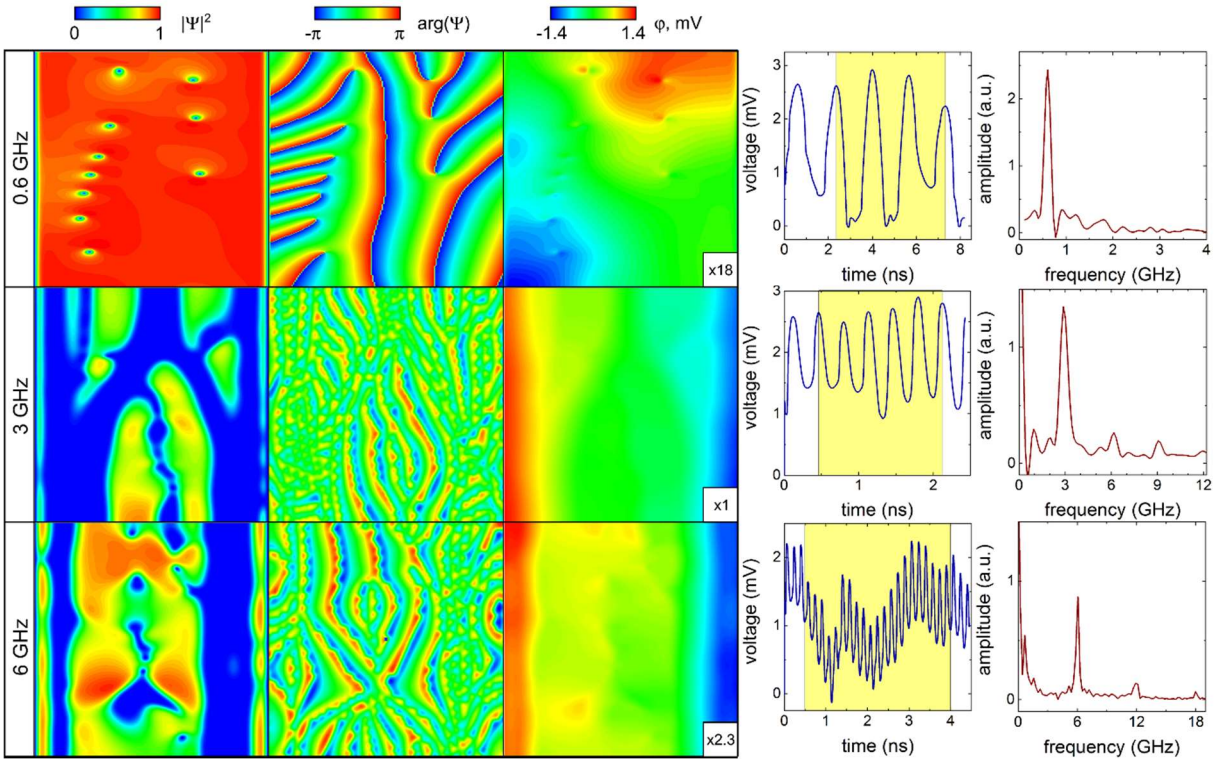

Fig. 5. Effect of the ac frequency on the dynamics of topological defects. Stationary stages of the evolution of the modulus and phase of the order parameter, electric potential, time-dependent voltage and its FFT for B= 2 mT at $\frac{j_1}{j_0} = 0.5$ and the ac frequencies 0.6, 3 and 6 GHz for open nanotubes listed in Table 2.

superconducting state in both half-cylinders around the region opposite to the slit, where there is a depression of the order parameter. Islands of superconductivity are also present near the banks of the slit. For the ac current frequency 3 GHz, the induced voltage as a function of time rather closely resembles the evolution of the modulated transport current. The stationary induced voltage oscillates around 2 mV. At the same time, for the higher ac current frequency 6 GHz, the induced voltage as a function of time clearly reveals a *superposition* of an oscillation around 1 mV at the same frequency and a slower oscillation around 1 mV at the frequency ~0.7 GHz, which seems to be a manifestation of the dynamics of phase slips in the regions near the banks of the slit.

3.5. Effect of the dc magnitude in the high-frequency regime

The high-frequency regime allows for a clear separation of the dynamics of the superconductor order parameter induced by the ac from the dynamics of superconducting vortices / phase slips in the dc, which occurs at lower frequencies (see [Fomin12a]). For the modulated transport current with a higher dc density $j_0 = 2.4556 \times 10^9$ Am^{-2} and $\frac{j_1}{j_0} = 1.0$ at an ac frequency of 60 GHz (this frequency is still notably smaller than the gap breakdown frequency in Nb at $0.77T_c$), the critical magnetic field occurs lower than 2 mT, so that the body of the open tube occurs in the normal state for all three magnetic field values (2, 6 and 10 mT), as illustrated in Supplementary Figure 2. The voltage drop across the open tube

occurs mainly due to a combination of the normal current and the contributions of moving phase-slip regions, what leads to high values of U_0 ~3.7 to 3.8 mV. As a consequence, the induced voltage is modulated with a dominant frequency 60 GHz equal to the frequency of the ac component of the transport current and the modulations depth $\frac{U_1}{U_0}$ slightly rising from 0.29 for 2 mT and 6 mT to 0.31 for 10 mT. This rise is due to increasing contributions of normal currents and phase-slip regions to the overall voltage across the open tube. At the same time, the critical magnetic field of one-dimensional superconductivity near the banks of the slit is higher than 10 mT, so that there survive continuous or island-like narrow regions of superconductivity, shown in the first column. Such regime is characterized by nonlinear dynamics of superconducting state with a clear development of odd harmonics of the dominant frequency with $\frac{U_3}{U_0}$ ~0.035 to 0.038. This kind of dynamics, which is manifested most clearly for the selected here higher frequency *f* = 60 GHz, takes place also at lower frequencies.

At a lower value of the dc current density 2.1048×10^9 Am^{-2} (Supplementary Figure 3), the spectrum of the FFT of the induced voltage is dominated by the first harmonic at the ac frequency of 60GHz. This is because the superconducting state is filling almost all area of the open tube, except very narrow regions in the vicinity of contacts. The occurrence and motion of vortices lead to an appreciable reduction of the constant part of the induced voltage U_0 because of increasing dissipation and to a significant decrease of the modulation depth of the induced voltage at the first harmonic: from $\frac{U_1}{U_0} =$ 1.444 at *B*=0 through $\frac{U_1}{U_0}$ =1.213 at *B*=6 mT to $\frac{U_1}{U_0} = 0.621$ at *B*=10 mT.

A cardinally different picture dynamics of the superconductor state develops at a lower dc density $j_0 = 2.1048 \times 10^9$ Am^{-2} and $\frac{j_1}{j_0} = 0.5$ at the same ac frequency of 60GHz. At a weaker transport current, the superconducting state fills almost the entire open tube, except for narrow stripes along the edges of the cut. These stripes occur owing to the boundary conditions (see Section 2), which describe the arrival of the electrons with the transport current through the normal electrodes and their gradual conversion into Cooper pairs when going further into the superconducting sample. Such a regime is characterized by a deeper (as compared with a higher dc density) modulation of the induced voltage due to the first harmonic $\frac{U_1}{U_0} \sim 0.6$ to 1.4 and nonlinear dynamics of the superconducting state with a stronger development of odd harmonics of the dominant frequency with $\frac{U_3}{U_0}$ ~0.05 to 0.10. In summary, at high frequencies of the ac current, the main shaping factor of the distribution of the order parameter and the pattern of the induced voltage is the dc strength.

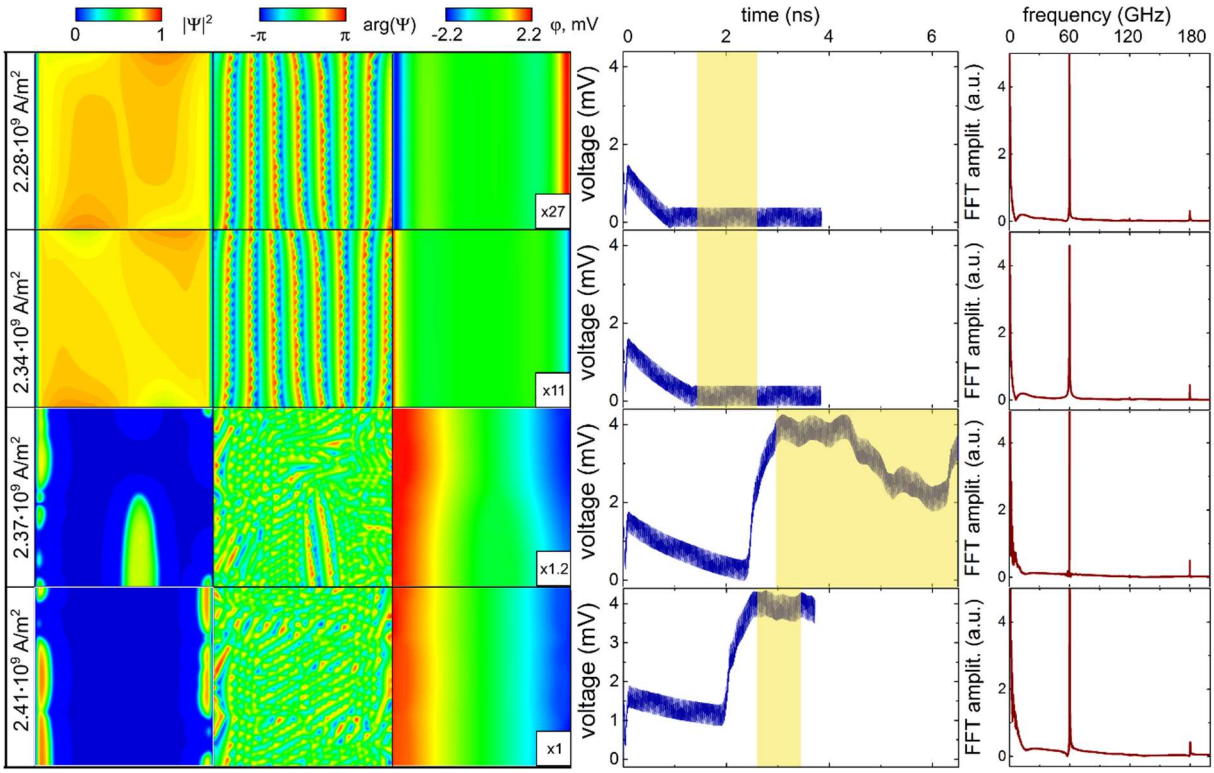

Fig. 6. DC-controlled transition between the two regimes in the superconducting state. Stationary stages of the evolution of the modulus and phase of the order parameter, electric potential, time-dependent induced voltage and its FFT at $B = 2$mT, $f = 60$ GHz for open nanotubes listed in Table 2 at a series of the dc magnitudes. The transition is practically completed at $j_0 = 2.411 \times 10^9$ Am^{-2}.

A transition between those regimes occurs at about between $j_0 = 2.324 \times 10^9$ Am^{-2} and $j_0 = 2.368 \times 10^9$ Am^{-2}(see Fig. 6) when the dynamics of the induced voltage remarkably reveals instability between the high values, typical of stronger dc, and the low values, typical of weaker dc. The FFT spectrum experiences a dramatic change, revealing an increase of $U_0 = 0.33$ mV [decreease of $\frac{U_1}{U_0} = 0.696$] for $j_0 = 2.324 \times 10^9$ Am^{-2} to $U_0 = 2.24$ mV [down to $\frac{U_1}{U_0} = 0.142$] for $j_0 = 2.368 \times 10^9$ Am^{-2}. The former case is characterized by the superconducting state filling in the whole open tube, excluding the normal regions along the contacts at the banks of the slit. The latter case reveals almost completely dominating phase slips, where the potential drops. The transition is practically completed for the transport current density $j_0 = 2.411 \times 10^9$ Am^{-2}, when U_0 is slightly increased up to 2.43 mV $\left[\frac{U_1}{U_0}\right.$ is slightly decreased down to $\left.0.123\right]$. The same patterns of the order parameter and the potential survive up to 2.456×10^9 Am^{-2}. This transition opens up a novel way to experimentally unveil the distributions of the order parameter through observation of the time-dependent induced voltage.

4. Discussion

The behavior of superconductivity in open nano/microtubes in a magnetic field orthogonal to the axis under a modulated (dc+ac) transport currents manifests a plethora of inhomogeneous states with distinct induced voltage-versus-magnetic field characteristics. The key effect is a transition between two regimes of superconducting dynamics. The first regime is characterized by a pronounced first harmonic in the FFT spectrum of the induced voltage at the frequencies of the ac current. It is typical of two limiting cases, when the dominant area of the open tube is superconducting at relatively low magnetic fields and/or weak dc currents or normal at relatively high magnetic fields and/or strong dc currents. The second regime is represented by a rich FFT spectrum of the induced voltage with pronounced multiple harmonics of the ac frequency the because of an interplay between the dynamics of superconducting vortices or phase slips and the dynamics induced by the ac. This finding implies unprecedented possibility to experimentally unveil the distributions of the order parameter through observation of the time-dependent induced voltage and to control the modulated transport in superconductor nano/microarchitectures.

The applicability of the model of 2D superconductor micro/nanoarchitectures analyzed in the present paper is highly realistic, because such structures have been successfully fabricated, e.g., from Nb [Lösch19], Nb-C [Porrati19] and W-C [Cordoba19]. Signatures of vortex and phase-slip patterns in nanohelices have been experimentally identified and supported by numerical simulations based on the TDGL equation [Cordoba19]. In those structures, the occurrence of imperfections (mechanical defects in self-rolled films and impurity atoms in 3D-written structures) must be taken into consideration in further research. Besides, real edge barriers for nucleation of superconducting vortices are not perfect (notches, materials composition variations etc). The quality of the barriers in superconductors is known to be decisive for the evolution of the order parameter in the entire sample [Dobrovolskiy2020]. However, the unveiled transitions between different configurations of topological defects governed by the global superconducting screening currents flowing over the entire structures are of topological nature and therefore robust with respect to defects and impurities.

The dissipative nature of the transport of vortices and phase-slip regions, which induce a resistive state of micro/nanoarchitectures, raises an important task of heat removal, especially in the regime of close-to-depairing transport currents. Solution to this problem can be twofold: (i) by adding a shunt resistance with $R < R_{tube}$ parallel to the open tube [Korneeva2020] or (ii) embedding the open tube directly into liquid helium. Among challenges to be met in further work, there is a *theoretical* one which is related to the (dc+ac)-driven escape of quasiparticles from the vortex cores, leading to the complex dynamics of vortices in a quasiparticle "cloud" in the form of additional phase-slip lines [Dob19pra] and *experimental* one, occurrence of spurious capacitances/inductances in the transmission line, which may significantly modify the overall shape of the observed $U(t)$, yet the FFT first-harmonic peaks should be expected to be clearly seen.

Conclusion

In conclusion, curved superconductor nano-/ microarchitectures (like open tubes and helical coils) allow for new, highly correlated vortex dynamics, novel phase-slip events and unprecedented topological transitions between them as compared to quasi-1D filaments and quasi-2D stripes. The topological transitions between vortex-chain and phase-slip transport regimes in curved superconductor micro/nanoarchitectures open up a possibility to efficiently tailor the superconducting properties of nanostructured materials by inducing a nontrivial topology of superconducting screening currents.

Additional information

Supplementary Materials accompany this paper.

Supplementary Materials

Supplementary Figure 1
Supplementary Figure 2
Supplementary Figure 3

Supplementary Video 1: Topological transitions in open superconductor nanotubes under a modulated transport current. 1 (figshare.com)

Supplementary Video 2: Topological transitions in open superconductor nanotubes under a modulated transport current. 2 (figshare.com)

Acknowledgements

V. M. F. acknowledges support from the DFG (Germany) under the Project # FO 956/6-1. O.V.D. acknowledges the Austrian Science Fund (FWF) for support through Grant No. I. 4889 (CurviMag). The authors acknowledge the ZIH TU Dresden for providing its facilities for high throughput calculations. This work was supported by the European Cooperation in Science and Technology via COST Action No. CA16218 (NANOCOHYBRI).

References

[Fomin18a] V. M. Fomin (Editor), *Physics of Quantum Rings*, Springer, Berlin - Heidelberg, 2014, 487 p.; *Physics of Quantum Rings*, 2nd Edition, Springer International Publishing, Cham, 2018, 586 p.

[Fomin18b] V. M. Fomin, *Topology-driven effects in advanced nanoarchitectures*, in: A. Sidorenko (Ed.), *Functional Nanostructures and Metamaterials*, Springer International Publishing, Cham, 2018, pp. 195 – 220.

[Makarov21] D. Makarov, O. M. Volkov, A. Kákay, O. V. Pylypovskyi. B. Budinska, O. V. Dobrovolskiy, New Dimension in Magnetism and Superconductivity: 3D and curvilinear geometry, Adv. Mater. 33, 2101758 (2021).

[Prinz00] V. Y. Prinz, V. A. Seleznev, A. K. Gutakovsky, A. V. Chehovskiy, V. V. Preobrazhenskii, M.A. Putyato, T. A. Gavrilova, Free-standing and overgrown InGaAs/GaAs nanotubes, nanohelices and their arrays. Physica E: Low-dimension. Syst. Nanostruct. 2000, 6, 828–831.

[Schmidt01a]. O. G. Schmidt, K. Eberl, Nanotechnology—Thin solid films roll up into nanotubes. Nature 410, 168 (2001).

[Fomin21] V. M. Fomin, Self-rolled Micro- and Nanoarchitectures: Topological and Geometrical Effects. De Gruyter, Berlin-Boston 148 pp. (2021).

[Little62] W. A. Little, R. D. Parks, Phys. Rev. Lett. 9, 9 -12 (1962).

[Moshchalkov95] V. V. Moshchalkov, L. Gielen, C. Strunk, R. Jonckheere, X. Qiu, C. Van Haesendonck, Y. Bruynseraede, Nature 373, 319-322 (1995).

[Tinkham63] M. Tinkham, Phys. Rev. 129, 2413–2422 (1963).

[Meservey72] R. Meservey, L. Meyers, Phase Transition of Thin-Film Superconducting Cylinders in a Magnetic Field. II. Angular Dependence. Phys. Rev. B 6, 2632–2642 (1972).

[Gladilin08] V. N. Gladilin, J. Tempere, I. F. Silvera, J. T. Devreese, V. V. Moshchalkov, Phys. Rev. B 77, 024512 (2008).

[Tempere09] J. Tempere, V. N. Gladilin, I. F. Silvera, J. T. Devreese, V. V. Moshchalkov, Phys. Rev. B 79, 134516 (2009).

[Carillo10] F-. Carillo, G. Papari, D. Stornaiuolo, D. Born, D. Montemurro, P. Pingue, F. Beltram, F. Tafuri, Phys. Rev. B 81, 054505 (2010).

[Zhao03] H. Zhao, V. M. Fomin, J. T. Devreese, V. V. Moshchalkov, Solid State Commun. 125, 59–63 (2003).

[Sochnikov10] I. Sochnikov, A. Shaulov, Y. Yeshurun, G. Logvenov, I. Božović, Nature Nanotechnology 5, 516–519 (2010).

[Lösch19] S. Lösch, A. Alfonsov, O. V. Dobrovolskiy, R. Keil, V. Engemaier, S. Baunack, G. Li, O. G. Schmidt, D. Bürger, Microwave Radiation Detection with an Ultrathin Free-Standing Superconducting Niobium Nanohelix. ACS Nano 13, 2948–2955 (2019).

[Pacheco20] A. Fernandez-Pacheco, L. Skoric, J. M. De Teresa, J. P. Navarro, M. Huth, O. V. Dobrovolskiy, Writing 3D nanomagnets using focused electron beams. Materials 13, 3774 (2020)

[Cordoba19] R. Córdoba, D. Mailly, R. O. Rezaev, E. I. Smirnova, O. G. Schmidt, V. M. Fomin, U. Zeitler, I. Guillamón, H. Suderow, J. M. De Teresa, Three-dimensional superconducting nanohelices grown by He+-focused-ion-beam direct writing, Nano Letters, Nano Lett. 19, 8597-8604 (2019).

[Orus2021] P. Orús, V. M. Fomin, J. M. De Teresa, R. Córdoba, Critical current modulation induced by an electric field in superconducting tungsten-carbon nanowires, Sci Rep 11, 17698 (2021).

[Dobrovolskiy2020] O. V. Dobrovolskiy, D. Yu. Vodolazov, F. Porrati, R. Sachser, V. M. Bevz, M. Yu. Mikhailov, A. V. Chumak, M. Huth, Ultra-fast vortex motion in a direct-write Nb-C superconductor, Nat. Commun. 11, 3291 (2020)

[Porrati2019] F. Porrati, S. Barth, R. Sachser, O. V. Dobrovolskiy, A. Seybert, A. S. Frangakis, and M. Huth, Crystalline niobium carbide superconducting nanowires prepared by focused ion beam direct writing, ACS Nano 13, 6287–6296 (2019)

[Fomin12a] V. M. Fomin, R. R. O. Rezaev, O. G. Schmidt, Tunable Generation of Correlated Vortices in Open Superconductor Tubes, Nano Lett. 12, 1282-1287 (2012).

[Rezaev14] R. O. Rezaev, V. M. Fomin, O. G. Schmidt, Vortex dynamics controlled by pinning centers on Nb superconductor open microtubes, Physica C 497, 1-5 (2014).

[Rezaev15] R. O. Rezaev, E. A. Levchenko, O. G. Schmidt, V.M. Fomin, Dynamics of the Abrikosov Vortices on Cylindrical Microtubes, Russian Physics Journal 58, 623-628 (2015).

[Rezaev16] R. O. Rezaev, E. A. Levchenko, and V. M. Fomin, Branching of the vortex nucleation period in superconductor Nb microtubes due to an inhomogeneous transport current, Supercond. Sci. Tech. 29, 045014, 1-7 (2016).

[Fomin17] V. M. Fomin, R. O. Rezaev, E. A. Levchenko, D. Grimm, O. G. Schmidt, Superconducting nanostructured microhelices, Journal of Physics: Condensed Matter 29, 395301, 1-9, (2017).

[Rezaev19] R. O. Rezaev, E. A. Posenitskiy, E. I. Smirnova, E. A. Levchenko, O. G. Schmidt and V. M. Fomin, Voltage Induced By Superconducting Vortices In Open Nanostructured Microtubes, Phys. Stat. Sol. RRL 13, 1-12 (2019).

[Rezaev20] R. O. Rezaev, E. I. Smirnova, O. G. Schmidt, V. M. Fomin, Topological transitions in superconductor nanomembranes in a magnetic field with submicron inhomogeneity under a strong transport current, Communication Physics 3, 144 (2020).

[Smirnova2020] E. I. Smirnova, R. O. Rezaev, V. M. Fomin, Simulation of dynamics of the order parameter in superconducting nanostructured materials: Effect of the magnetic field renormalization, Low Temperature Physics 46, 325–330 (2020).

[Pompeo08] N. Pompeo and E. Silva, Reliable determination of vortex parameters from measurements of the microwave complex resistivity, Phys. Rev. B 78, 094503 (2008).

[Dobrovolskiy15a] O. V. Dobrovolskiy and M. Huth. Dual cut-off direct current-tunable microwave low-pass filter on superconducting Nb microstrips with asymmetric nanogrooves. Appl. Phys. Lett. 106, 142601 (2015).

[Fiory71] A.T. Fiory, Quantum Interference Effects of a Moving Vortex Lattice in Al Films, Phys. Rev. Lett. 27, 501 (1971).

[Martinoli75] P. Martinoli, O. Daldini, C. Leemann, E. Stocker, A.C. Quantum interference in superconducting films with periodically modulated thickness. Solid State Commun 17, 205 (1975).

[Shklovskij14] V. A. Shklovskij, V. V. Sosedkin, and O. V. Dobrovolskiy. Vortex ratchet reversal in an asymmetric washboard pinning potential subject to combined dc and ac stimuli. J. Phys.: Condens. Matter 26, 025703 (2014).

[Dobrovolskiy15b] O. V. Dobrovolskiy, M. Huth, and V. A. Shklovskij. Alternating current-driven microwave loss modulation in a fluxonic metamaterial. Appl. Phys. Lett. 107, 162603 (2015).

[Dobrovolskiy20b] O. V. Dobrovolskiy, E. Begun, V. M. Bevz, R. Sachser, and M. Huth. Upper frequency limits for vortex guiding and ratchet effects. Phys. Rev. Appl. 13, 024012 (2020).

[Thurmer08] D. J. Thurmer, C. Deneke, O. G. Schmidt, In situ monitoring of the complex rolling behaviour of InGaAs/GaAs/Nb hybrid microtubes, J. Phys. D: Appl. Phys. 41, 205419, 1-5 (2008).

[Thurmer10] D. J. Thurmer, C. C. Bof Bufon, C. Deneke, O. G. Schmidt, Nanomembrane-based mesoscopic superconducting hybrid junctions, Nano Lett. 10, 3704-3709 (2010).

[Dobrovolskiy12] O. V. Dobrovolskiy, M. Huth, Crossover from dirty to clean superconducting limit in dc magnetron-sputtered thin Nb films, Thin Solid Films 520, 5985-5990 (2012).

[Tinkham96] M. Tinkham, Introduction to Superconductivity, McGraw-Hill, New York, 1996, 454 pp.

[Gropp96] W. D. Gropp, H. G. Kaper, G. K. Leaf, D. M. Levine, M. Palumbo, V. M. Vinokur, Numerical Simulation of Vortex Dynamics in Type-II Superconductors, J. Comput. Phys. 123, 254-266 (1996).

[Dobrovolskiy20c] Private communication (2020).

[Mayadas1972] A. F. Mayadas, R. B. Laibowitz, and J. J. Cuomo, Journal of Applied Physics 43, 1287 (1972)

[Gubin2005] A. I. Gubin, K. S. Il'in, S. A. Vitusevich, M. Siege, N. Klein, Phys. Rev. B 72, 064503 (2005).

[Kato93] R. Kato, Y. Enomoto, S. Maekawa, Effects of the surface boundary on the magnetization process in type-II superconductors, Phys. Rev. B 47, 8016-8024 (1993).

[Kogut79] J. B. Kogut, An introduction to lattice gauge theory and spin systems, Rev. Mod. Phys. 51, 659-713 (1979).

[Saad96] Y. Saad, Iterative Methods for Sparse Linear Systems, Second Edition, Society for Industrial and Applied Mathematics (SIAM), Philadelphia, 2003, 547 pp.

[Korneeva20] Yu. P. Korneeva, N. N. Manova, I. N. Florya, M. Yu. Mikhailov, O. V. Dobrovolskiy, A. A. Korneev, D. Yu. Vodolazov. Different single photon response of wide and narrow superconducting MoSi strips, Phys. Rev. Appl. 13, 024011 (2020).

[Dob19pra] O. V. Dobrovolskiy, V. M. Bevz, E. Begun, R. Sachser, R. V. Vovk, and M. Huth. Fast dynamics of guided magnetic flux quanta. Phys. Rev. Appl. 11, 054064 (2019).

Supplementary Files

This is a list of supplementary files associated with this preprint. Click to download.

- Supplementary.pdf
- figS1.png
- figS2.png
- figS3.png